THEORY OF BASIN SCALE DYNAMICS OF A STRATIFIED ROTATING FLUID

LEO R.M. MAAS
Netherlands Institute for Sea Research, P.O. Box 59, 1790 AB Texel, The Netherlands
E-mail: maas@nioz.nl

(Received 10 December 2001; Accepted 4 March 2004)

Abstract. The dynamics of a stratified fluid contained in a rotating rectangular box is described in terms of the evolution of the lowest moments of its density and momentum fields. The first moment of the density field also gives the position of the fluid's centre-of-mass. The resulting low-order model allows for fast assessment both of adopted parameterisations, as well as of particular values of parameters. In the ideal fluid limit (neglect of viscous and diffusive effects), in the absence of wind, the equations have a Hamiltonian structure that is integrable (non-integrable) in the absence (presence) of differential heating. In a non-rotating convective regime, dynamically rich behaviour and strong dependence on the single (lumped) parameter are established. For small values of this parameter, in a self-similar regime, further reduction to an explicit map is discussed in an Appendix. Introducing rotation in a nearly geostrophic regime leads through a Hopf bifurcation to a limit cycle, and under the influence of wind and salt to multiple equilibria and chaos, respectively.

Keywords: center-of-mass dynamics, diffusionless Lorenz equations, liquid pendulum, Shil'nikov phenomenon, uniformly-rotating stratified fluid

1. Introduction: Moments characterising the state of a basin

The first question of a physicist, entering the field of lake and ocean dynamics may despite some holiday experiences be: '' what is a lake, and what is an ocean''? A limnologist or oceanographer might refer to a certain reservoir of water, having in some frame of reference its geometric centre at O, being of dimensions $L \times B \times H$, containing fluid characterized by state variables S_n $(n = 1, 2, 3, \ldots)$, such as its temperature, salinity, flow, etc., and exchanging heat, water, solutes, momentum, etc., with the outer world through its boundaries B_n at rates Q_n (river input and output, evaporation and precipitation, insolation, wind-stress, etc.). Clearly, we usually cannot simply do with just one single value of any such state-variable, since these are all *fields*, quantities that depend on both space and time in a continuous way. A common way of proceeding is by monitoring just the temporal change of certain *integral* measures of these fields, their ''moments'' (e.g., Fisher et al., 1979). Taking for instance some substance's

Surveys in Geophysics **25:** 249–279, 2004.

concentration S as general state variable, supposed to vary only in the x-direction, an integral measure of this substance is simply the total amount (total "mass") present in the lake (or ocean):

$$M_S(t) = \int S(x,t)\,\mathrm{d}x, \tag{1}$$

the integral extending over the length of the lake. A first description of the mass *distribution* is offered by weighting the concentration with the position, giving the position of the centre-of-mass of substance S as

$$X_S(t) = \frac{1}{M_S}\int xS(x,t)\,\mathrm{d}x. \tag{2}$$

With reference to the power with which position x appears in these integrals, these two quantities are referred to as the zeroth and first moments of substance S, respectively. Higher order moments, obtained by multiplying the concentration field with x^n (for integer $n > 1$) and integrating over the domain, give information about the spreading of mass around the origin (or around its centre-of-mass, when multiplying S with $(x - X_S)^2$), the skewness of this spread, etc.. These notions can quickly be generalized to three dimensions. Here we restrict consideration to a rectangular basin of size $L \times L \times H$, which is temperature-stratified only, in which, by assumption, the zeroth order moments of mass and heat are fixed (so that there is no net evaporation or precipitation, nor any net river input or output, and neither a net heating nor cooling). The container is assumed to be in steady, uniform rotation (on an f-plane). We thus conceive the appealing idea that the dynamics of the position vector of its centre-of-mass may to some extent be representative of the basin-scale dynamics of a mid-latitude lake or sea (Morgan, 1956; Maas, 1994).

The moments method was used previously to describe, e.g., the figure of the Earth under the influence of self-gravitation and rotation (Chandrasekhar, 1968), and the collective motion of fluids that are linearly stratified in temperature (Dolzhanskiy, 1977) and additionally in salt (Holm, 1978). The linear spatial dependence of temperature and salt fields employed therein will be adopted here too. The resulting low dimensional set of ordinary differential equations, describing the evolution of the amplitudes of these moments, is related to similar low-order systems that can be obtained by a Galerkin projection of the partial differential equations onto a set of modes that satisfy equations and boundary conditions (Lorenz, 1960; Obukhov, 1969; Obukhov and Dolzhansky, 1975; Dolzhanskiy and Pleshanova, 1983). Such equations have also been interpreted as describing

(forced and damped) coupled gyrostats, where a single gyrostat is a gyroscope (a rotating body in a uniform field of gravity) subject to additional torques due to rotation, stratification, etc., and is described by a triplet of nonlinearly coupled equations that conserve energy and phase volume (Gluhovsky and Dolzhanskiy, 1980; Gluhovsky, 1993; Gluhovsky and Agee, 1997).

There are physical as well as mathematical reasons for reducing the full dynamics of a set of coupled fields governed by the Navier–Stokes equations in the Boussinesq approximation to a severely truncated system (represented here by the dynamics of their lowest moments). Physically, this is motivated by the presence of an inverse energy cascade: both rotation as well as stratification lead to a pile-up of energy at the largest scales (Lesieur, 1996). Mathematically, this is because low-order models can be used quickly to explore a (restricted) parameter space with relative ease (Olbers, 2001). This is an attractive property, lost in more sophisticated numerical models that usually contain a large number of parameters that specify geometry, forcing, as well as parameterisations and discretisations needed to make the governing equations amenable to numerical analysis, whose influence cannot so readily be assessed. In such cases, typically one's physical intuition is invoked to decide which of these parameters can be assumed to be fixed, and which represent an absence of knowledge on our part, whose impact therefore needs to be established by a (generally crude) stepwise variation. The numerical integrations are then assumed to capture possible bifurcations that might take place in between the steps, and to depend smoothly on the unresolved parameters. This bypasses the question of whether these assumptions are actually correct. The sensitive dependence on the only remaining parameter in a worked-out example, below, shows that this may be quite erroneous.

It is important to notice that a basin need not (and in general will not) have its centre-of-mass at the geometric centre. In fact, this happens only in the isothermal–isohaline case. In a motionless, stably-stratified fluid, for instance, gravity will displace the centre-of-mass directly below the geometric centre, its distance to this centre being representative of the degree of stratification. Only when this distance recedes to zero, does the fluid reach the isothermal state. When the centre-of-mass is far below the geometric centre, the stratification is very stable. This distance can also be regarded as the length of an equivalent fluid pendulum (Figure 1) whose motion, under the influence of differential buoyancy sources, will be our main concern here. Note that, in distinction to a traditional pendulum, the fluid pendulum is able to change its length by moving its ''mass point'' in any arbitary direction under the influence of external forcing as, e.g., surface cooling or heating.

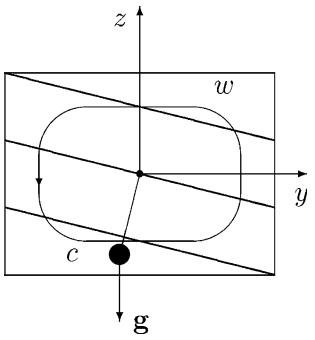

Figure 1. Schematic of a (planar) fluid pendulum, describing the motion of a heated, stratified fluid confined to a rectangular box. Straight lines denote sloping isotherms, whose distance (stratification rate) is inversely proportional to the length of the fluid pendulum, the distance between the centre-of-mass (large dot) and geometric centre (small dot). Warm and cold fluid is indicated by w and c, respectively. The sense of motion of the pendulum, depicted by the direction of small arrow, is determined by the gravitational (buoyancy) torque $\mathbf{g}$ (thick arrow).

2. Dynamics of centre-of-mass

The motion of an incompressible, viscous fluid on a rotating f-plane is governed by the Navier–Stokes equations. In the Boussinesq approximation these read

$$\frac{\mathrm{D}\mathbf{u}}{\mathrm{D}t} + f\mathbf{k}\times\mathbf{u} = -\nabla p - \rho g\mathbf{k} + \nabla\cdot(\mathbf{A}\nabla\mathbf{u}), \tag{3}$$

$$\nabla\cdot\mathbf{u} = 0, \tag{4}$$

$$\frac{\mathrm{D}\rho}{\mathrm{D}t} = \nabla\cdot(\mathbf{K}\nabla\rho), \tag{5}$$

where $\mathrm{D}/\mathrm{D}t = \partial/\partial t + \mathbf{u}\cdot\nabla$. Here $\mathbf{u} = (u, v, w)$ denotes the vector of the velocity components along the three Cartesian $\mathbf{x} = (x, y, z)$ axes, of which the vertical z component is antiparallel to gravity. The Coriolis parameter is denoted as f, and $\mathbf{k}$ is a vertical unit vector. The pressure, p, and density, ρ', are scaled perturbation quantities: $p = (p_* - p_0)/p_0$, $\rho' = (\rho_* - \rho_0)/\rho_0$, where the starred quantities denote the original, dimensional quantities, ρ_0 is the constant (average) reference density with which a pressure p_0 is hydrostatically related, and g denotes the acceleration of gravity. Eddy viscosity and diffusivity are denoted by tensors A_{ij} and K_{ij}, respectively, considered to consist of (constant) diagonal terms, differing only in the

horizontal and vertical (subscripts h, v) directions. At the boundaries these equations are supplemented with appropriately prescribed fluxes of momentum, or buoyancy (heat/salt).

We assume that the time scale $T = L^2/K_h$ is set by diffusion. Because we consider an application to a rectangular box of size $L \gg H$ in the x and z directions, respectively, we scale these directions and their velocities correspondingly:

$$[x, z, u, w, p] = [L, H, K_h/L, HK_h/L^2, (K_h/L)^2]. \tag{6}$$

Scaling in the y-direction follows that in x. With this scaling the box has unit sizes (centred on the origin). We shall further assume that the buoyancy field (here considered to represent solely and monotonically the temperature field) $g\rho' = R\rho$, with an as yet undetermined magnitude R. The dimensionless density field is assumed to be given by a polynomial expansion

$$\rho = 12[xX(t) + yY(t) + zZ(t)] + (x^2 - 1/12)\sigma_X(t) + \cdots, \tag{7}$$

so that the density perturbation has no net mass ($\int \rho \, \mathrm{d}V = 0$), and to lowest order consists of plane surfaces (of arbitrary orientation and strength), whose basin-averaged density gradient $\overline{\nabla\rho} \equiv \int_V \nabla\rho \, \mathrm{d}V = 12\mathbf{X}$ is proportional to the location of the centre-of-mass $\mathbf{X} = (X, Y, Z) = \int_V \mathbf{x}\rho \, \mathrm{d}V$. Here V denotes the volume of the basin (and $\mathrm{d}V$ a volume increment), and σ_X measures mass-spreading. Up to a multiplication factor, Z is sometimes interpreted as the potential energy in a field of gravity (Staquet, 2000). Note that the expansion of the density field is such that neither the low-order moments are affected by higher order moments (e.g., the volume integral of $\mathbf{x}$ times a higher order term, such as $(x^2 - 1/12)$, vanishes), nor are its lowest basin-averaged derivatives affected by its higher derivatives (e.g., the basin average of $\nabla\rho$ is independent of σ_X). This allows us to consider the evolution of the lowest order moments separately, as we do here. Restricting our attention to the biggest scales of motion is also loosely motivated by the fact that rotation and stratification impose a kind of two-dimensionality on the fluid, that, under turbulent forcing (not resolved here), evokes an up-scale transport of energy: the "inverse energy cascade" (Sommeria, 1986; Rutgers, 1998).

The evolution equation of, e.g., the X component of the centre-of-mass is obtained by multiplying the diffusion equation by x and by adding $\rho(\mathrm{d}x/\mathrm{d}t - u) = 0$, which vanishes because of the definition of u. We obtain

$$\frac{\mathrm{d}(x\rho)}{\mathrm{d}t} - u\rho = x\nabla \cdot (\mathbf{K}\nabla\rho).$$

Next, inserting the expansion for ρ in the inertial and advective terms and integrating over the basin, the following considerations can be made. The first term yields $\mathrm{d}X/\mathrm{d}t$. The second term contains

$$\int_V xu\,\mathrm{d}V = \int_V x\frac{\mathrm{d}x}{\mathrm{d}t}\,\mathrm{d}V = \int_V \frac{1}{2}\frac{\mathrm{d}x^2}{\mathrm{d}t}\mathrm{d}V = \frac{1}{2}\frac{\mathrm{d}}{\mathrm{d}t}\left(\int_V x^2\mathrm{d}V\right) = 0 \tag{8}$$

which vanishes, as it can be rewritten as the time-derivative of a geometrically fixed quantity. Here integration and differentiation interchange because the basin is of fixed size. (Formally, this requires noting that, on employing the continuity equation, the advective term can be written as the divergence of a flux whose volume integral vanishes because the normal component of the flow vanishes at the boundaries.) In another term,

$$\int_V 2yu\mathrm{d}V = \int_V\left(y\frac{\mathrm{d}x}{\mathrm{d}t} - x\frac{\mathrm{d}y}{\mathrm{d}t}\right) + \left(y\frac{\mathrm{d}x}{\mathrm{d}t} + x\frac{\mathrm{d}y}{\mathrm{d}t}\right)\mathrm{d}V, \tag{9}$$

the second part of the right hand side vanishes for the same reason. The first part of the right hand of (9), however, is identified as the vertical component $-L_3$ of the basin-averaged angular momentum vector $\mathbf{L} = 6\int_V \mathbf{x}\times\mathbf{u}\,\mathrm{d}V$, whose dynamics clearly needs separate consideration.

The diffusive term, $\int_V x(\partial_x K_h\partial_x + \partial_y K_h\partial_y + \partial_z K_v\partial_z)\rho\,\mathrm{d}V$, can be simplified with a partial integration and use of the prescribed boundary conditions. Assuming that the diffusive fluxes $K_h\rho_x$ through the East (E) and West (W) vertical boundaries vanish, the first term yields

$$-K_h\int_V \rho_x\mathrm{d}V + \int\int xK_h\rho_x\,|_W^E\,\mathrm{d}y\mathrm{d}z = -12K_hX, \tag{10}$$

using (7) in the first integral. This diffusive term thus acts as "Newtonian cooling". In the absence of diffusive fluxes through the northern and southern vertical boundaries, the middle term $\int_V x\partial_y K_h\rho_y\,\mathrm{d}V$ vanishes. The last term $\int_V x\partial_z K_v\rho_z\,\mathrm{d}V$ can be partially integrated in the vertical, and, with a prescribed heat flux through the surface $K_v\rho_z = Q(x,y)$ (and none at the bottom), it represents differential zonal heating: $F^{(x)} \equiv \int\int xQ\,\mathrm{d}x\mathrm{d}y$.

In order to close the equations we need to know how the basin-averaged angular momentum vector evolves. Its evolution is obtained by taking the cross-product of $\mathbf{x}$ with the momentum equation and integrating over the basin. Since $\mathbf{x}\times\mathrm{d}\mathbf{u}/\mathrm{d}t = \mathrm{d}(\mathbf{x}\times\mathbf{u})/\mathrm{d}t$, the integral $\int_V \mathbf{x}\times\mathrm{d}\mathbf{u}/\mathrm{d}t\,\mathrm{d}V = \mathrm{d}\mathbf{L}/\mathrm{d}t$. Remarkably, the non-linear advective terms vanish identically. The torque by the pressure gradient force can be written as a surface integral, which vanishes under the assumption that there is no anisotropic external pres-

sure torque acting on the fluid (Holm, 1986) (see Appendix A). This leads to a very small value of the scale R. Assuming, however, that the density field is to first approximation hydrostatic leads to a more acceptable scale, larger than the previous one by a factor equal to L^2/H^2. The horizontal pressure gradient field then reads $-(p_x, p_y) = -12gRz(X, Y)$, which gives rise to a buoyancy torque term $gR(Y\mathbf{i} - X\mathbf{j})$, with $\mathbf{i}$ and $\mathbf{j}$ unit vectors in the x and y directions. This provides the coupling to the dynamics of the centre-of-mass. The viscous terms, finally, can be treated in a way similar to the diffusive terms, and lead to side-wall, bottom and internal frictional terms, together captured in a Rayleigh damping $\propto -L_i (i = 1, 2, 3)$. The terms that represent a flux of "differential momentum" through one of the boundaries, the external torque, such as, e.g., that due to the wind stress τ at the surface ($z = 1/2$), or as mediated by the Ekman boundary layer at the base of the mixed layer (Appendix A), give

$$\mathbf{T} = \int\int \left(-\frac{1}{2}\tau^{(y)}, \frac{1}{2}\tau^{(x)}, x\tau^{(y)} - y\tau^{(x)} \right) \mathrm{d}x\mathrm{d}y. \tag{11}$$

Together, we obtain a system of six equations (Maas, 1994) coupling the dynamics of the basin-averaged angular momentum vector $\mathbf{L}$ to that of the centre-of-mass, $\mathbf{X}$ forced by differential momentum $\mathbf{T}$ and buoyancy $\mathbf{F}$ fluxes, subject to the Earth's rotation ($f' = f/2r_h$), friction ($r = r_v/r_h$) and diffusion ($\mu = K_v L^2/K_h H^2$). Here, $r_{h,v}$ represent Rayleigh damping coefficients in the horizontal and vertical directions.

$$Pr^{-1}\frac{\mathrm{d}\mathbf{L}}{\mathrm{d}t} + f'\mathbf{k} \times \mathbf{L} = -Y\mathbf{i} + X\mathbf{j} - (L_1, L_2, rL_3) + \hat{T}\mathbf{T}, \tag{12}$$

$$\frac{\mathrm{d}\mathbf{X}}{\mathrm{d}t} + \mathbf{X} \times \mathbf{L} = -(X, Y, \mu Z) + Ra\,\mathbf{F}. \tag{13}$$

In these equations we find $Ra = g\delta\rho_e H/2r_h K_h \rho_0$, a Rayleigh number, indicative of the forcing strength, $\hat{T} = u_*^2 L/2r_h K_h H$, giving the magnitude of the wind stress torque, and $Pr = r_h L^2/12K_h$, a Prandtl number, measuring the ratio of a diffusive L^2/K_h to a viscous r_h^{-1} time scale. A final rescaling of time with a factor $1/12$, angular momentum and centre-of-mass coordinates (both with a factor 2) has been applied. This leads to a density scale $R = 12r_h K_h/gH$ in terms of which the external density contrast, $\delta\rho_e$, related to the differential heating, is measured in the Rayleigh number. We also assume that a frictional velocity, $u_* = |\tau|^{1/2}$ is known. Note that we have here adopted an f-plane, assuming that the (effective) background rotation axis is determined by the projection of the Earth's

rotation vector along the vertical, so that, at latitude ϕ, $f\hat{\mathbf{k}} = \Omega \sin(\phi)\hat{\mathbf{k}}$. In certain cases, particularly near the equator, one may wish to use its unprojected version Ω instead. In the following we look at some limiting cases of (12) and (13).

Note that Eqs.(12) and (13) represent a version of the virial equations (Chandrasekhar, 1968) adapted to the Boussinesq description of a fluid, in which inertial mass density (as opposed to heavy mass density) is replaced by a constant. In the present case these equations have been extended with viscous and diffusive damping terms, and, owing to the fixed confinement of the fluid, have been analysed with respect to the differential motions only (no steady translation of centre-of-mass).

3. Ideal fluid limit: Hamiltonian structure

Neglecting diffusive and viscous terms (setting $\mathbf{K} = \mathbf{A} = 0$, see (3) and (5)), we consider the dynamics of an ideal rotating, uniformly stratified fluid in response to forcing. Here we assume this to be due solely to differential heating in the meridional (y) direction $\mathbf{F} = (0, 1, 0)$, and consider the wind to be absent ($\mathbf{T} = 0$). Eq. (12) shows that the horizontal circulation (as presented by L_3) is then a constant, taken to be zero here. Without loss of generality we have set the Prandtl number, Pr, and Coriolis parameter f equal to one, as these can be scaled out in this limit. Thus (12) and (13) reduce to the following five coupled equations describing the evolution of angular momenta in the meridional-vertical plane $l \equiv L_1$, the zonal–vertical plane $m \equiv L_2$ and the centre-of-mass $\mathbf{X} = (X, Y, Z)$:

$$\begin{aligned} &\dot{l} - m = -Y \\ &\dot{m} + l = X \\ &\dot{X} - Zm = 0 \\ &\dot{Y} + Zl = Ra \\ &\dot{Z} + Xm - Yl = 0, \end{aligned} \tag{14}$$

Inserting X and Y from the first two of these into the last equation reveals a first integral of motion, denoted as B

$$B \equiv Z + (l^2 + m^2)/2, \tag{15}$$

whose constant value is determined by the initial values of Z, l and m. Inserting X and Y into (14c, d) yields

$$\begin{aligned} &\ddot{m} + \dot{l} - Zm = 0 \\ &\ddot{l} - \dot{m} - Zl = -Ra, \end{aligned} \tag{16}$$

where, from (15),

$$Z(l, m) = B - (l^2 + m^2)/2. \tag{17}$$

With $r = \dot{l},\ s = \dot{m}$, these equations can be written as

$$\begin{aligned} \dot{l} &= H_r \\ \dot{m} &= H_s \\ \dot{r} &= -H_l + H_s \\ \dot{s} &= -H_m - H_r, \end{aligned} \tag{18}$$

with

$$H \equiv \frac{1}{2}(r^2 + s^2 + Z(l, m)^2) + Ra\, l. \tag{19}$$

This is a two degrees-of-freedom, generalized Hamiltonian system (Zaslavsky et al., 1991) with coordinate-momentum pairs (l, r) and (m, s), respectively. The Hamiltonian H consists of a quadratic kinetic part $T = (r^2 + s^2)/2$ and a quartic potential part $V(l, m) = Z^2/2 + Ra\, l$, with $Z(l, m)$ given by (17). (Choosing the first momentum differently, as $r = \dot{l} - m$, these equations obtain the canonical Hamiltonian form (O. Bokhove, personal communication).) The Hamiltonian is a second integral of motion that is conserved during evolution, reducing the dynamics to that of three coupled ordinary differential equations. For two values of the Hamiltonian, the resulting three equations are numerically integrated for $Ra = 1$. In a Poincaré section Figure 2 shows the typical structure of elliptic and hyperbolic fixed points, periodic orbits and, revealing the non-integrability for this value of Ra, stochastic webs. When the forcing vanishes ($Ra = 0$), an additional integral of motion ($D \equiv (X^2 + Y^2 + Z^2)^{1/2}$) exists, the radius of the equivalent fluid pendulum. In that case, the Hamiltonian system is integrable. The KAM theorem predicts that most of the periodic orbits persist when this integrable Hamiltonian is slightly perturbed (Zaslavsky et al., 1991). This is still visible in the Poincaré section of Figure 2(b), for a large Hamiltonian perturbation ($Ra = 1$).

Hamiltonian flow conserves phase space volume. This extends even to the mapping in the Poincaré section, which is area-preserving. Obviously,

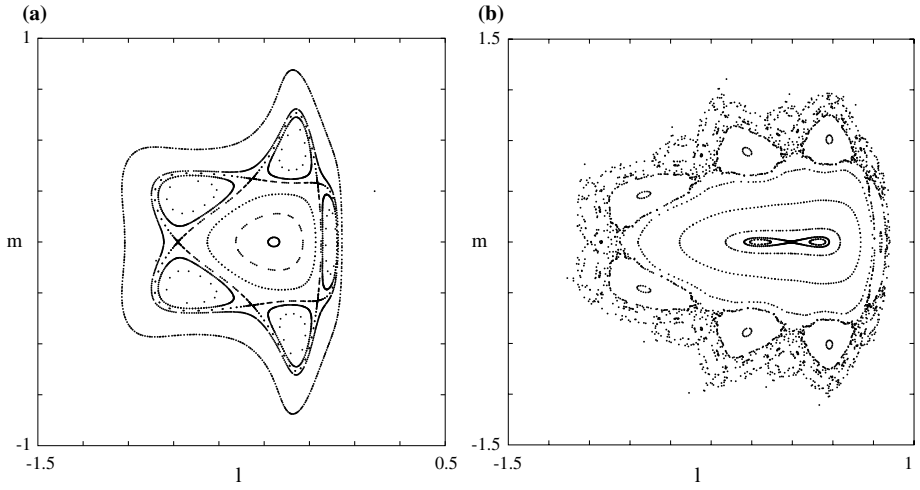

Figure 2. Poincaré section at $s = 0$ for $\dot{s} < 0$ of numerical integration of the Hamiltonian equations in the phase plane spanned by the angular momenta (l, m) for $B = 0$, $Ra = 1$ and energy level (a) $H = 0$, and (b) $H = 1$.

this property is lost when viscous effects are introduced. Phase space now contracts and much of the irregularity, and even periodic orbits are generally lost. However, under certain circumstances, these flows can still be chaotic as will be shown in some examples in the next section. Further study is needed to elucidate the impact of the ideal fluid's Hamiltonian structure on the viscous equations, with whose study we now proceed under other simplifying assumptions.

4. Convective case: differential vertical buoyancy fluxes

As convection by vertically differing buoyancy fluxes in the ocean or lakes is usually a relatively small-scale feature, we defer discussion of the effect of rotation to Section 5.2. When wind and rotation are absent ($\hat{T} = f' = 0$) in (12) and (13) the dynamics in two orthogonal vertical planes decouple. Let there be a perhaps externally preferred horizontal direction, y say, to which plane the motion is confined. Then, reorienting the coordinate system correspondingly, the motion is represented by a single component of the angular momentum vector $L \equiv L_1$, and the governing equations reduce to

$$Pr^{-1}\dot{L} + Y = -L \tag{20}$$

$$\dot{Y} + LZ = -Y \tag{21}$$

$$\dot{Z} - LY = -\mu Z + Ra. \tag{22}$$

Here we look at convection driven by differential vertical buoyancy forces (along the direction of gravity) so that it is assumed that $F^{(x)} = F^{(y)} = 0$ and $F^{(z)} = 1$ (its strength being absorbed in the definition of the Rayleigh number). When there is no motion ($L = 0$), the centre-of-mass is exactly below the geometric centre ($Y = 0$), and the resulting dynamics simply reflects the effect of diffusion and differential heating (terms on the right-hand side of (22)).

Diffusion moves the centre-of-mass towards the geometric centre (raising it, when it is initially below it (see Staquet, 2000), forcing drives it to unstable stratification, $Z > 0$, when $Ra > 0$ (or stable stratification, $Z < 0$, when $Ra < 0$). As soon as the centre-of-mass is slightly off-axis ($Y \neq 0$), however, macroscopic motion $L \neq 0$ starts to develop, and the three coupled equations (20)–(22) determine its evolution (Figure 3).

Apart from a translation and re-orientation of the vertical coordinate ($Z \to Ra/\mu - Z$), these equations are identical to the celebrated Lorenz equations (Lorenz, 1963), where they emerge as a highly truncated set of coupled Fourier modes. But, with reference to the direction of gravity, this implies that the Lorenz equations are "upside down". Also, the explicit nature of the forcing in (20)–(22) makes their physical meaning more transparent. The constant term Ra is, of course, simply the applied heating/cooling. In the convective case, heating at the bottom drives the centre-of-mass upwards, above its stable level ($Z = 0$). Angular momentum is then generated by the buoyancy torque (second term of the first equation), when it is not exactly above this centre (i.e., it has a slight off-axis component $Y \neq 0$, or, alternatively, has some initial angular momentum $L \neq 0$). This

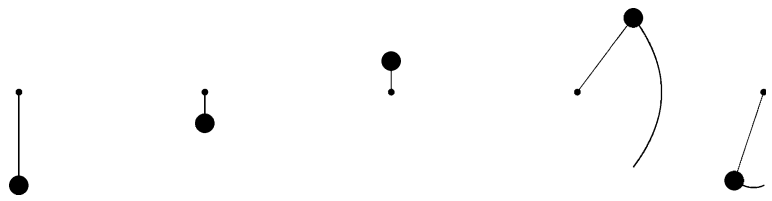

Figure 3. Schematic of the *dynamics* of a fluid pendulum. From left to right: slow, nearly vertical (and axial) rise of the centre-of-mass (thick dot) under the influence of heating, followed by sudden and fast overturning, and a few quickly damped relaxation oscillations to a new stable location, again nearly below the geometric centre (thin dot).

moves the centre-of-mass downwards (second terms of second and third equations). The damping terms, on the right, represent mechanical friction, $-L$, and diffusion $-(Y, \mu Z)$, respectively. Diffusion tries to move the centre-of-mass back to the geometric centre, while friction removes momentum, and, as a consequence, the liquid pendulum may at times be nearly stuck to a certain off-axis position $Y \neq 0$ when its angular momentum is effectively drained. Notice that the present derivation has no spectral leakage (such as that due to the truncation of a Fourier expansion). Owing to the linear space dependence of the temperature and salinity fields, projection leads to a natural decoupling of the dynamics of the lowest moments (as considered here) from those of higher order.

While the remaining three equations thus possess the richness, known from the extensively studied Lorenz equations (Sparrow, 1982), the fact that this system still contains three parameters (viz. Pr, μ, Ra) makes it too difficult to study comprehensively. The difficulties encountered when exploring our own three-dimensional physical space (almost entirely restricted to a thin band over the surface of our planet) illustrates that scanning a three dimensional parameter space is not an easy task. For that reason it is worthwhile searching for still more simple models within (20)–(22). Apart from pragmatic reasons there are also mathematical and physical motives to attempt a further simplification. A sound mathematical adage may well be that new insight is obtained by simplifying a problem as much as one can, without "trivializing" it ("trivial" here referring to all pre-existing knowledge). Physically, there is also a good reason, as these equations contain just one source but two "sink" terms (viz. friction and diffusion), and it is thus natural to enquire what happens when just one of these damping mechanisms dominates. We can achieve this by rescaling (20)–(22), such that a parameter appears in front of either the diffusive terms, or the friction term. Taking that parameter to be small (zero), we obtain a reduced set of equations, which we may then try to solve. If we thus eliminate the friction term, the remaining equations can be integrated, but the angular momentum then grows indefinitely. This is in conflict with the assumptions underlying the scaling, so that we consider this scaling to be self-invalidating. It is left as an exercise for the reader to find the rescaling and solution of the reduced set of equations.

4.1. The diffusionless lorenz equations (DLE)

When, however, the diffusive terms are eliminated by scaling $(L, Y, Z) \to Pr(L, Y, Z)$, $t \to t/Pr$, and by taking both $Pr, Ra \to \infty$, such that $R = Ra/Pr^2$ remains finite, the solutions do *not* blow up (when Y and L do not simultaneously vanish). We refer to this single-parameter set as

the Diffusionless Lorenz Equations (DLE, see van der Schrier and Maas, 2000):

$$\dot{L} = Y - L \tag{23}$$

$$\dot{Y} = LZ \tag{24}$$

$$\dot{Z} = -LY + R. \tag{25}$$

Their solutions (e.g., Figures 4 and 5) display the typical richness known from the full Lorenz equations, exhibiting (for R decreasing from ∞ downwards) period-doubling bifurcations leading to chaos (characterised by positive Lyapunov exponent, Figure 6(a)), a strange attractor (at, e.g., $R \approx 1$, Figure 6(b)), symmetry breaking bifurcations, multiple equilibria and Shil'nikov's phenomenon (Sparrow 1982; van der Schrier and Maas, 2000). The latter is associated with the presence of a homoclinic orbit to a fixed point of the saddle-focus type at special values $R = R_s$. As R approaches any of these R_s, from below or above, the periodic cycle undergoes an *infinite* number of saddle-node bifurcations. Hence the curve depicting this periodic equilibrium in parameter space shows a spiral roll-up, where the cycle in phase space resembles the homoclinic orbit more and more as R_s is approached. Moreover, the cycle also exhibits an infinite number of period-doubling bifurcations. Due to the presence of these

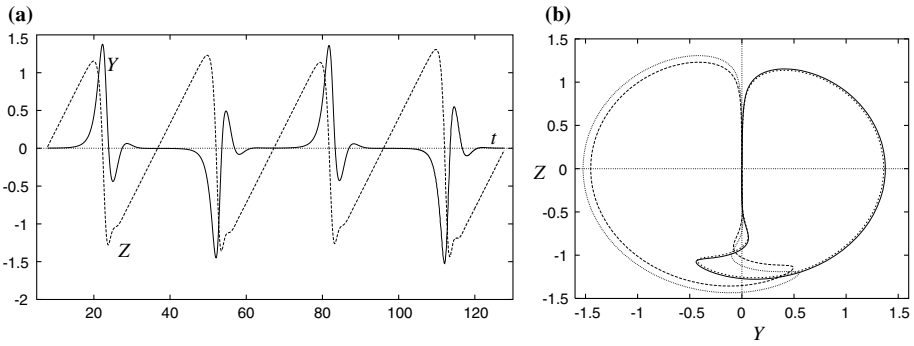

Figure 4. (a) Horizontal Y (solid) and vertical Z (dashed) coordinates of the centre-of-mass as a function of time t following from a numerical integration of the Diffusionless Lorenz Equation (DLE) for $R = 0.1$ over four subsequent cycles of subsequent duration $T_{1,\ldots,4}$. (b) $Y - Z$ phase plane (here identical to real space) representing the same curves. Different dashings indicate different subsequent cycles. Longer durations T result in larger lengths of the fluid pendulum (distance to the geometric centre).

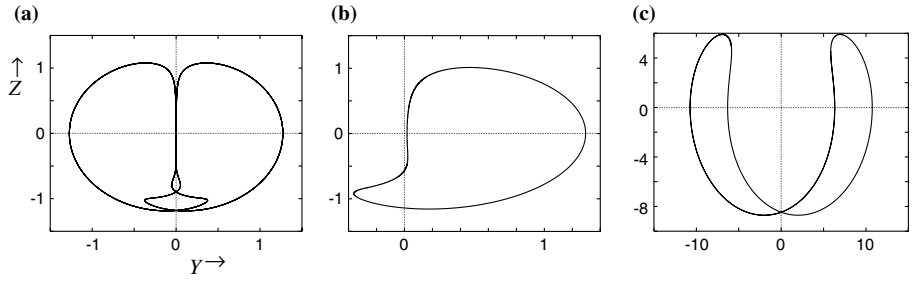

Figure 5. Phase plane $Y - Z$ representations of numerical integrations of the DLE for R equal to (a) 0.08, (b) 0.135, (c) 10. (taken from van der Schrier and Maas, 2000).

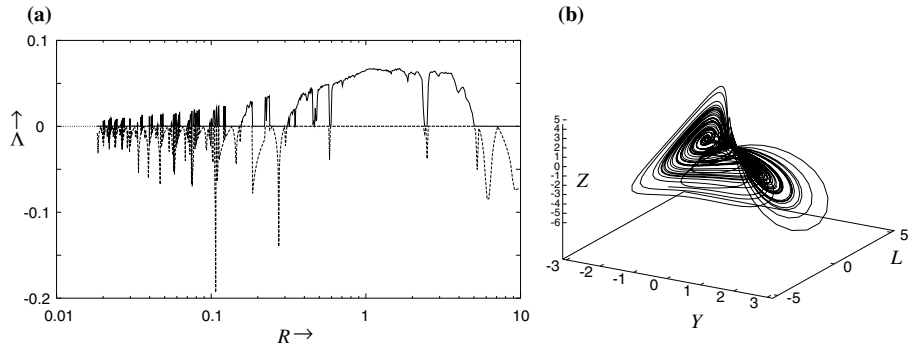

Figure 6. (a) Two largest Lyapunov exponents Λ (solid and dashed, respectively) as a function of R for the DLE (taken from van der Schrier and Maas, 2000). (b) Numerical integration of the DLE for $R = 1$.

period-doubling and saddle-node bifurcations, the curve in parameter space frequently changes its stability (Glendenning and Sparrow, 1984; Mullin and Price, 1989).

4.2. Self-similar behaviour

Paradoxically, the structure seems to be still richer, as, in contrast to the full Lorenz equations, the DLE display a self-similar behaviour as $R \ll 1$, in which all of the previous behaviour is echoed in repetitively smaller parameter windows (Figure 7). (This reflects Shil'nikov's phenomenon, showing that periodic states successively lose stability and "fall" onto a neighbouring branch). Moreover, an approximate analytical solution can be obtained in this part of parameter space, recovering this dependency, which will be sketched here. Notice that this self-similar, chaotic behaviour

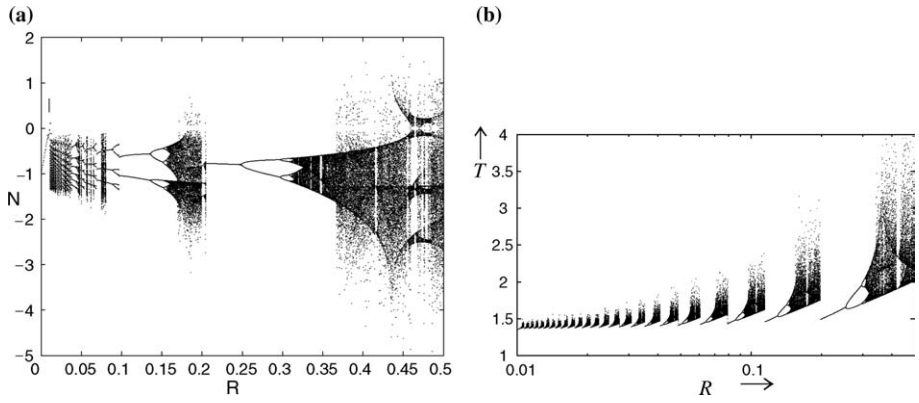

Figure 7. (a) Poincaré section, giving the Z-position at $Y = 0$, of numerically integrated DLE for a number of different R, ranging from 0.01 (vertical line) to 0.5. (b) Bifurcation diagram of the duration T of successive cycles obtained by iterating a map derived from the DLE for varying R (taken from van der Schrier and Maas, 2000). Notice the difference in the abscissae.

for infinitesimally small values of R is quite remarkable, as it implies that regular perturbation theory, by means of which we might otherwise be inclined to tackle (23)–(25), always leads to erroneous results. This perturbation approach assumes that we can develop the dependent variables in convergent power series of R, e.g., as $L(t;R) = L_0(t) + RL_1(t) + R^2L_2(t) + \cdots$. Notice, however, that $R(\ll 1)$ is now acting as an *ordering* parameter, whose precise (small) value can no longer matter. In other words, in this approach L, Y and Z are assumed to depend smoothly on R, an assumption defied by the numerical and analytical results, no matter how small R actually is. Sensitive dependence of the solution no longer applies to just the initial conditions, but also to the parameter. It suggests that for $R \ll 1$ the DLE are invariant under some as yet unknown similarity transformation. The reader may verify that a regular perturbation solution of (23)–(25) signals that there are "problems", by again leading to unbounded growth of its higher order terms.

For $R \ll 1$, the "fluid pendulum" exhibits the following behaviour. Most of the time it resides very close to the vertical axis ($|Y| \ll 1$), being almost depleted of angular momentum ($|L| \ll 1$), slowly raising its centre-of-mass under the (weak) external forcing. Then, when this is above the geometric centre, it is formally unstable. Yet, the instability needs time to grow – the longer so, the closer the pendulum is to the axis. Then, at some point, the gravitational (buoyancy) torque sets in, and the pendulum quickly moves downward, dropping below its geometric centre, almost without receiving further buoyancy, fixing its length (distance to the origin), where it oscillates a few times in fairly viscous surroundings, so

that it quickly sticks at a different distance from the axis, perhaps also on the other side of it, from which point the cycle starts again (see Figure 3). The latter relaxation oscillation and the former sudden growth of the angular momentum and subsequent drop of the pendulum are both well described by a linear (Airy) equation. The only nonlinearity left is in the duration T' over which this equation applies, which sensitively depends on the previous distance to the axis, directly related to the duration of the previous cycle T (determining the "length" which the fluid pendulum could acquire). We can thus construct (see Appendix B) what turns out to be an analytical multi-peaked map that relates the duration of one cycle to that of the next (Figure 8). This compares qualitatively (and to some extent quantitatively) with a numerically determined multi-peaked map (Lorenz, 1979). From this map we determine (multiple) fixed points as the intersections with the bisector, and their stability from the slope of the map at these intersections. Iterating the map (Figure 7(b)) shows period doubling and chaos in a number of self-similar windows that decrease in size with decreasing R. As this map "compresses" (the peaks becoming closer) when R decreases, this reveals Shil'nikov's phenomenon in yet another way. Figure 8 illustrates how intersections (equilibria) may disappear through a tangent bifurcation, as seen at $T \approx 1.35$, creating a sudden jump to a still

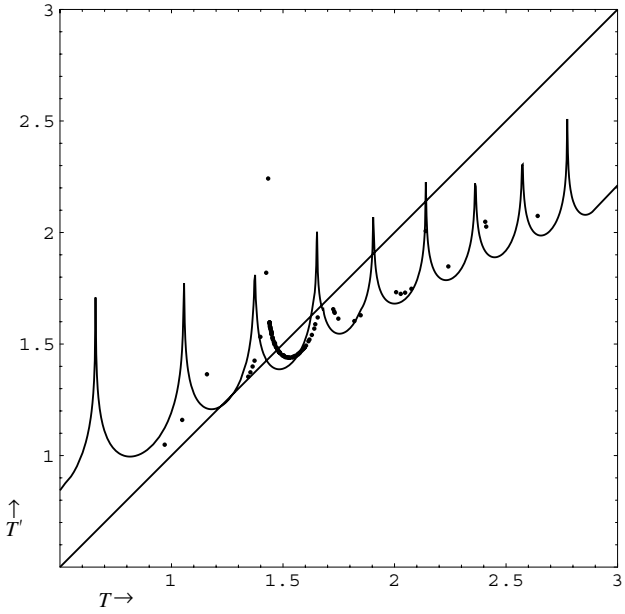

Figure 8. Analytical map $T'(T)$, the cusped solid line given by Eq. (43), and numerical iterations of DLE (dots) for $R = 0.1$. The solid sloping line presents the bisector.

existing equilibrium. An implicit form of a multi-peaked map for the full Lorenz equations is derived by Fowler and McGuinness (1982, 1983).

5. Differential lateral buoyancy fluxes and extensions

A midlatitude sea may be mainly driven by lateral differences in buoyancy fluxes, e.g., those due to incoming short-wave solar radiation at low latitudes, compensated by a heat loss in the form of long-wave radiation at high latitudes, so that we here assume that $F^{(y)} = 1, F^{(x)} = F^{(z)} = 0$. Note that, in a lake, river inflow and outflow may mimic such a situation. When the Prandtl number is assumed to be large, (12) simplifies, and the overturning circulation (described by its angular momentum L) is frictionally balancing the torque due to the basin-averaged, latitudinal buoyancy gradient, $L = -Y$. When the vertical diffusion is again strong compared with the horizontal ($\mu \gg 1$), also the inertia in the last equation, controlling the vertical position of the centre-of-mass, may be eliminated (by assuming that $Y \to \mu Y$ and by taking the limit $\mu \to \infty$), so that, in terms of the original variables, the lateral buoyancy gradient (Y) is governed by

$$\dot{Y} = Ra - Y - L^2 Y/\mu. \tag{26}$$

5.1. Adding salt

In its present form (26) is – dynamically – not very interesting. Each initial density contrast will veer towards the equilibrium described by the vanishing of its right hand side. However, the dynamics becomes richer when the density contrast Y is assumed to be also determined by lateral salt-differences, S, instead of just temperature differences T, so that the linearized equation of state yields $Y = -T + S$ (after rescaling with the thermal and haline expansion coefficients). In particular, when the salt has its own dynamics, either due to having a different restoring time scale, or due to a different exchange with the atmosphere, multiple steady states can be anticipated to occur. This relates to the multiple equilibria of the thermohaline circulation as found in box models in which the circulation in a midlatitude ocean is conceived as the flow between two adjacent boxes, representing the sub-equatorial and sub-polar regions (Stommel, 1961). In the present case, both T and S are (approximately) governed by eq. (26), except that Ra and μ refer to different constants $Ra_{T,S}$ etc, for heat and salt, respectively. Steady states are obtained by the vanishing of the right hand sides of these equations, and by subtracting the resulting equations, replacing the difference $T - S$ by L, one algebraic equation for L is obtained:

$$L = \frac{Ra_T}{1 + L^2/\mu_T} - \frac{Ra_S}{1 + L^2/\mu_S}. \tag{27}$$

By graphical inspection this is seen to possess multiple steady states (for appropriate parameter values), retrieving Stommel's (1961) finding in a box model. The last term in (26) represents advection, or, in box-model terminology, the exchange flow between the two boxes. Stommel (1961) argued that the exchange should be insensitive to the sense of the circulation (sign of L) and thus took its modulus $|L|$. The present reduction from the Navier-Stokes equations confirms this *ad hoc* argument, recovering the insensitivity to the sense of the circulation through its squared appearance L^2 (Maas, 1994; van der Schrier and Maas, 1998).

5.2. Adding rotation

Large lakes and oceans are affected by rotation, so that it is worthwhile to examine its effect, initially on an f-plane, by taking $f' \neq 0$ in eq. (12). Since we intend to keep the equations manageable, we shall make the same ansatz that $Pr \to \infty$, removing the inertia from the angular momentum equations. With this assumption, and an intermediate rescaling $(X, Y, Z, Ra) \to (1 + f'^2)(X, Y, Z, Ra)$, we find:

$$L_1 = -Y + f'X \tag{28}$$

$$L_2 = X + f'Y, \tag{29}$$

which, when $f' \to \infty$, represent geostrophic relations, and

$$L_3 = \frac{\hat{T}}{r}. \tag{30}$$

Dropping the wind for the moment, so that $L_3 = 0$, assuming vanishing zonal differential buoyancy fluxes $F^{(x)} = 0$, and inserting the remaining angular momenta in the equations for the centre-of-mass, we obtain (Maas, 1994):

$$\dot{X} = (X + f'Y)Z - X \tag{31}$$

$$\dot{Y} = (Y - f'X)Z - Y + RaF^{(y)} \tag{32}$$

$$\dot{Z} = -\mu Z - (X^2 + Y^2) + RaF^{(z)}. \tag{33}$$

These equations are identical to another model, which Lorenz proposed as "possibly the simplest atmospheric general circulation model", in which Z denotes the strength of the jet-stream, and X and Y the sine and cosine components of a long planetary wave (Lorenz, 1984, 1990). Lorenz showed that these equations exhibit chaos when $F^{(z)}$ is large. (For a more extensive bifurcation analysis, see van Veen, 2002). In oceans, or large-scale lakes, lateral differential buoyancy fluxes are presumably more important, so that we shall again consider the case $F^{(y)} = 1, F^{(z)} = 0$.

By setting the right hand sides equal to zero, we obtain $(X, Y) = Ra(f'Z, 1 - Z)/((1 - Z)^2 + f'^2Z^2)$. When inserted in the last equation (at equilibrium) this yields

$$Z((1 - Z)^2 + f'^2Z^2) = -Ra^2/\mu. \tag{34}$$

Because the right hand side is negative, there is always just one statically stable ($Z < 0$) steady state, which implies that $X < 0$, $Y > 0$ and, from these, a thermal circulation with north-eastward ($L_1 < 0, L_2 > 0$) surface flow. This flow may, however, become unstable for certain values of the rotation rate (f'), diffusivity (μ) and forcing (Ra). We may check this by perturbing the solution around that at steady state, found above, with $(X', Y', Z')e^{\nu t}$ and, upon substitution into eq. (33) and linearisation, derive the cubic equation for the eigenvalue ν. For small values of the parameter all three eigenvalues have negative real parts, and the equilibrium is stable. But at some parameter setting two eigenvalues cross the real axis simultaneously, $\nu = \pm ib$, and a periodic solution (limit cycle) results (Hopf bifurcation), without, however, violating the static stability ($Z < 0$ always).

Again, adding salt, the resulting equations may show a still richer behaviour, up to chaos in the salt-dominated regime. On the other hand, the Stommel-type of multiple equilibria may cease to exist when rotation increases (van der Schrier and Maas, 1998).

6. Effect of wind

We wish to add a wind stress field, supposed to represent the mid-latitude wind pattern, with its high-latitude westerlies and low-latitude easterlies. This is here condensed to the assumption that it exerts a constant negative torque, $T^{(z)} = -1$ (its magnitude being represented by $\hat{T}$), leading in a steady state, by (30), to a uniform horizontal circulation, represented by a

negative constant $L_3 < 0$. Equations similar to (33) result, except for the replacement of $f'Z \to f'Z - L_3$ in the two first equations. The steady states are again governed by (34), provided the same replacement is made there too:

$$h(Z) \equiv Z((1-Z)^2 + (f'Z - L_3)^2) = -Ra^2/\mu. \tag{35}$$

Multiple equilibria may now arise again (in the absence of any salt stratification) due to the combined effects of rotation and wind. They require, first of all, $h(Z)$ to be non-monotonic. By requiring its derivative $\mathrm{d}h/\mathrm{d}Z = 0$ to vanish, we determine (with $w \equiv \sqrt{3}$) when its roots

$$Z_\pm = \frac{2(1+f'L_3) \pm [((L_3 - w)f' + 1 + wL_3)((L_3 + w)f' + 1 - wL_3)]^{1/2}}{3(1+f'^2)} \tag{36}$$

are real, see Figure 9(a). For the northern hemisphere, $f' > 0$. Since $h(Z)$ is an asymptotically increasing function of Z and since we require the local minimum to be negative (in order for it to equal the negative quantity $-l^2 \equiv -Ra^2/\mu$), multiple equilibria occur for cases that $h(Z_+) < 0$.

For each $f' > w$ and $L_3 < -w$, this occurs for $f' > f'_+ \equiv (wL_3 - 1)/(L_3 + w)$, over some interval of Rayleigh numbers (l^2), see Figures 9(b) and (c). Conditions for the instability of these equilibria can be derived along the lines discussed for the windless case in Section 5 (see Maas, 1994).

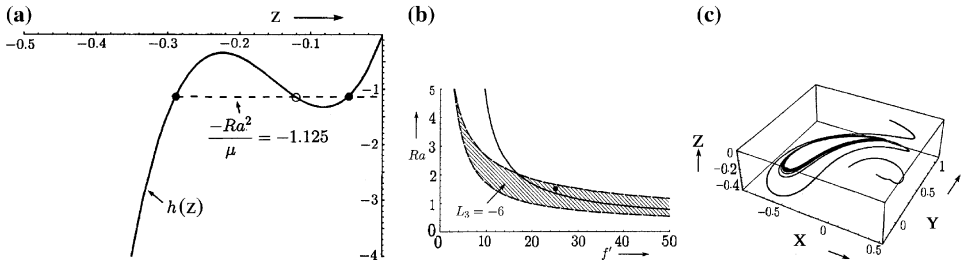

Figure 9. (a) Equilibrium curve $h(Z)$, for $f' = 25, \mu = 2$, showing multiple equilibria (solid circle: stable, open circle: unstable) due to having three intersections with the (dashed) line $l^2 = Ra^2/\mu =$ constant. (b) For $\mu = 2$ and for wind-induced, horizontal circulation having $L_3 = -6$, multiple equilibria exist in the dashed region of the $Ra - f'$ parameter plane. Crossing the solid line from below, one of the previous stable equilibria turns unstable via a Hopf bifurcation. The dot indicates the parameter values used in the X, Y, Z-phase space (identical to physical space) of (c) displaying these two equilibria: a stable fixed point, and a limit cycle, circling around the (now unstable) equilibrium. The initial positions are denoted by a dot.

7. Discussion and summary

The density field of a continuously stratified rotating fluid contained in an enclosed basin can be expanded in a global Taylor series, a series of orthogonal polynomials. Their time-dependent amplitudes are equivalent to the moments of the density field. Assuming that there is a balance between net buoyancy gain and loss, the leading term, the average density excess, vanishes. The lowest *dynamic* moment, the basin-averaged density gradient, is a vector that can also be interpreted as the fluid's centre-of-mass position relative to the geometric centre. Owing to a peculiarity of the non-linearities in hydrodynamic systems (namely that these are quadratic), this first order moment of the density field evolves independently of the higher order moments (but not the reverse!). This allows us to neglect higher order moments (describing the density field's spread, skewness, etc.), particularly as both stratification and rotation provide a degree of two-dimensionality to the fluid that, under turbulent forcing (not modelled here), through a so-called inverse energy cascade, leads to a pile up of energy at the largest scales.

The first moment of the density field is here solely determined by the first order moments of the buoyancy and momentum fluxes through the boundaries, and couples dynamically to the lowest non-trivial moment of the momentum field, the basin-averaged angular momentum. This results in a set of ordinary differential equations governing the centre-of-mass position vector and the basin-averaged angular momentum vector, Eq. (12)–(13), and has been employed here for just a few cases.

With relatively little effort a number of interesting submodels can be derived from it, under certain conditions displaying rich dynamics (nonintegrable Hamiltonian structure of the ideal fluid limit, and multiple steady states, limit cycles, bifurcations and strange attractors in a damped version). It can be extended with an independently varying salt field, and thus be used to test parameterisations in thermohaline circulation modeling by, e.g., linking a virtual salt flux to the local temperature instead of prescribing it externally (van der Schrier and Maas, 1998; van der Schrier, 2000). It can also be used to explore other boundary conditions, such as considering the effect of stochastic forcing representing weather variability (Monahan, 2002). Its versatility also makes it an interesting model to use in simplified ocean-atmosphere climate models (especially in its quasi-geostrophic limit), either of deterministic (van Veen, 2002; van Veen et al., submitted for publication) or stochastic (Arnold et al., 2002) nature. It finally seems attractive for use in a post-processing phase, compressing 3-D information obtained in field, laboratory or numerical experiments. In the field, undersampling probably makes this very hard to accomplish. In controlled laboratory and numerical experiments, however, this may well be the most succinct way of

expressing the state of a stratified, rotating fluid, and may help to provide a framework for interpreting the sparse field data.

Extending the model to an equatorial box, aimed at understanding the possible transition of an equatorially symmetric to asymmetric response under equatorially symmetric forcing, shows that some of the simplicity is lost, since higher order moments and some truncation come into play. However, this may be balanced by an increased insight into the symmetry breaking aspects due to three-dimensionality and the Earth's rotation (van der Schrier et al., unpublished manuscript).

Acknowledgements

The author is grateful to Joël Sommeria and Peter Davies for their kind invitation to present some lectures at the Grand Combin Summer School on "The fluid dynamics of coastal seas, closed basins and lakes". He is also greatly indebted to Gerard van der Schrier for comments and for preparing some of the figures, and to Uwe Harlander, Yonghui Wu and Joël Sommeria for comments on an earlier draft.

Appendix A: Details of derivation of moments model (12) and (13)

Here, we give arguments for the treatment of the pressure term in the moments model. Also, we discuss the moments of the viscous term $\int_V \mathbf{x} \times \nabla \cdot \mathbf{A}\nabla\mathbf{u}\,\mathrm{d}V$. Rather than simply replacing these viscous terms by Rayleigh damping $-r\mathbf{L}$, we show that there is room for distinguishing damping acting on the horizontal circulation (embodied in $-r_v L_3$) from that acting on the vertical circulations ($-r_h(L_1, L_2)$).

A.1. Pressure torque

When we consider the linearized 2-D equations in the Boussinesq approximation, taking the curl of the momentum equation eliminates the pressure gradient term. Thus we are left with two equations for streamfunction and buoyancy which can be simplified to an internal wave equation. When this equation is solved, subject to certain initial and boundary conditions, the pressure field can then be determined. Taking the divergence of the momentum equation, the pressure field is described by a Poisson equation, in which the vertical buoyancy gradient acts as a body force, that can then be considered as known. However, the solution of this Poisson equation requires that we specify the pressure (Dirichlet condition) or its normal

derivative (Neumann condition) at the boundary. If this is done anisotropically, this effectively operates as an *additional* (in this case, boundary) forcing mechanism. This may be relevant when we consider the response to surface waves at a free surface (Morgan, 1956), or to atmospheric pressure loading (Wunsch and Stammer, 1997). But, when considering the response to differential heating, there is no reason to prescribe an anisotropic externally imposed pressure field at the boundary. In the same sense, it is natural to again choose the pressure isotropic in the boundary pressure torque term of the equation governing the basin-averaged angular momentum. The effect of this choice will be that this torque term vanishes (while the interior pressure field will, of course, not). If, however, we aim to study the effects of free surface waves, or of atmospheric pressure loading, an anisotropically prescribed pressure at the surface simply acts as an additional forcing term in the moment equations too.

In the main text hydrostatic balance was assumed in the vertical momentum equation. This gave rise to an internally determined pressure field whose torque could be evaluated and led to the scaling of the density perturbation as given. Without a basic hydrostatic state, but retaining the requirement that there is no net external pressure torque, the same set of equations is obtained, but with a density scale reduced by a factor $(H/L)^2$, in terms of which any externally "applied" density contrast (as embodied in the definition of *Ra*) will be huge.

A.2. Viscous damping

The equations for the basin-averaged angular momentum result from taking the cross product of the position vector with the momentum equation, and subsequent integration over the whole (box-shaped) fluid domain V. Here we look more closely at the viscous term, yielding $\mathbf{S} \equiv \int_V \mathbf{x} \times \nabla \cdot \mathbf{A} \nabla \mathbf{u} \mathrm{d}V$. Expanding this, we find, e.g., as its vertical component

$$\hat{\mathbf{k}} \cdot \mathbf{S} = \int_V x[\partial_x(A_h v_x) + \partial_y(A_h v_y) + \partial_z(A_v v_z)] - y[\partial_x(A_h u_x) + \partial_y(A_h u_y) + \partial_z(A_v u_z)]\mathrm{d}V. \tag{A1}$$

This acts to drive and damp the horizontal circulation, represented by the vertical component of the angular momentum vector L_3, as can be seen by the partial integrations, use of boundary conditions and some closure assumptions.

We regard the fluid domain to consist of a (nearly) inviscid interior, up to the edge of a thin boundary layer adjacent to the rigid walls. Integration is assumed to extend up to this layer, where stresses relate by some stress law to the local velocity at the edge of this boundary layer: $A_n \partial_n u = s_n u$, allowing for some slip (see, e.g., Maas and Van Haren, 1987, using tidal observations from the North Sea). Here n refers to the inward normal direction, and s_n is a friction velocity. At the surface this stress is exerted by the wind stress $A_v(u_z, v_z) = \tau = (\tau_1, \tau_2)$.

Collecting z-derivatives and performing the integration from bottom (B) to top (T), yields an integral over the horizontal surface A : $\int_A (xA_v v_z - yA_v u_z) \mid_B^T \mathrm{d}A = \int_A (x\tau_2 - y\tau_1)_T - s_v(xv - yu)_B \,\mathrm{d}A$. This contains the torque of the wind stress at the top as a driving term, and a bottom friction term. We are tempted to close the description by relating the integral over the bottom area to that of the same quantity over the total volume divided by the depth:

$$-\int_A s_v(xv - yu)_B \,\mathrm{d}A \approx -\frac{s_v}{H}\int_V (xv - yu)\,\mathrm{d}V \equiv -\sigma_v L_3, \tag{A2}$$

introducing a decay rate $\sigma_v = s_v/H$.

Partial integrations of the remaining terms in (A1) from West (W) to East (E), or from South (S) to North (N) yield the following terms

$$\int_A (xA_h v_x - yA_h u_x) \mid_W^E + (xA_h v_y - yA_h u_y) \mid_S^N \mathrm{d}A + \int_V A_h(u_y - v_x)\mathrm{d}V. \tag{A3}$$

The first two terms are, of course, surface integrals over different side walls (indicated by E,W,etc.). In the first term of the first integral the stress law can be employed $A_h v_x = \pm s_h v$ (and similarly in the second term of the second integral), where the sign accounts for the derivative pointing inwards $(+)$ or outwards $(-)$. Employing the continuity equation to replace $u_x = -(v_y + w_z)$ in the second term of the first integral, and performing additional partial integrations on these two terms, in the y and z directions, respectively, yields, from the condition that there is no flow normal to the respective boundaries ($v_N = 0$, etc.):

$$-\int_A yA_h u_x \mid_W^E \mathrm{d}A = \int_A yA_h(v_y + w_z) \mid_W^E \mathrm{d}A = -\int_A A_h v \mid_W^E \mathrm{d}A. \tag{A4}$$

Hence, together with a similar term from the second integral of (A3), and a partial integration of the volume integral in (A3), we obtain the following, additional side-wall friction terms:

$$\int_A (-(|x|s_h + 2A_h)v\,|_W^E + (|y|s_h + 2A_h)u\,|_S^N)\mathrm{d}A. \qquad (A5)$$

Note that at the respective side walls, $|x| = L/2$, etc., are simply constant, so that (A5) equals $(Ls_h/2 + 2A_h)\int_A(-v\,|_W^E + u\,|_S^N)\mathrm{d}A$. The integral presents the horizontal circulation along the side wall. This can be also written as the volume integral of the vertical vorticity component, so that we shall again be tempted to close (A5) as being proportional to $-\sigma_h L_3$. Together with the bottom friction (A2), we obtain a damping $-r_v L_3$, with $r_v = \sigma_h + \sigma_v$. Note that the damping rate r_v, given the derivation, has an empirical character.

Similar arguments can be used also to close the horizontal components of **S**. We shall parameterise the damping terms acting on the horizontal angular momenta as $-r_h(L_1, L_2)$, retaining, by using a different subscript, only the possibility that the decay rate acting on these two terms is different from that acting on the horizontal circulation. The forcing of circulations in meridional and zonal vertical planes due to windstress is no longer by its *torque*, but rather, directly, by the net windstress itself (see (11)), assumed to vanish in this study.

Appendix B: Derivation of multipeaked map from DLE (19)

In van der Schrier and Maas (2000) the single parameter (R) Diffusionless Lorenz Equations (23)–(25) (DLE) were derived. It was shown that for $R \ll 1$ these equations are approximately solved by a second order Airy equation, which is applicable over a duration that depends on that of the preceding cycle. An alternative derivation is given here, leading to a qualitatively similar multi-peaked map, which, however, makes less assumptions in its derivation and whose peaks are located closer to those obtained by numerical integration.

In his seminal paper on deterministic non-periodic flows, Lorenz (1963) derived three nonlinearly coupled differential equations describing convection between two horizontal plates. While its numerically determined solutions show irregular transitions of positive to negative cycles of its dependent variables, the height of subsequent maxima of each of these cycles seemed to be strongly related to that of its predecessor. A plot of subsequent maxima against each other was shaped like a single peak tent, to which it was subsequently idealized. For such a map the (sensitive) chaotic dependence of iterations (depending on the initial conditions) could be established, and was rigorously linked to a symbolic shift map. In a later numerical integration, Lorenz (1979) observed that for other values of the

parameters, such a map could exhibit multiple peaks. An implicit map for the three parameter Lorenz equations was described in Fowler and McGuinness (1982, 1983). Here we follow van der Schrier and Maas (2000) by taking the one parameter diffusionless Lorenz equations (23)–(25), and obtain an explicit map.

The derivation starts with the observation that, for, $|L|, |Y| \ll R^{1/2}$, the vertical coordinate of the centre-of-mass, $Z \approx Rt + c$, where c is a constant of integration, which we take to be zero, so that time is measured from the moment that the centre of mass passes the geometric centre. Eliminating Y from the first two equations, and substituting this approximation for Z, leads to

$$\ddot{L} + \dot{L} - RtL = 0. \tag{B1}$$

For $L = \mathrm{e}^{-t/2}\tilde{L}$, and $\tau = \delta(t + 1/4R)$, with $\delta \equiv R^{1/3}$, we find that this reduces to the Airy equation:

$$\ddot{\tilde{L}} - \tau\tilde{L} = 0, \tag{B2}$$

where a dot now denotes a τ-derivative, so that the general solution reads

$$L = \mathrm{e}^{-\frac{1}{2}t}(\alpha \mathrm{Ai}(\tau) + \beta \mathrm{Bi}(\tau)), \tag{B3}$$

where Ai, Bi denote Airy functions (e.g., (Abramowitz and Stegun, 1965), and α and β are undetermined amplitudes. These solutions apply over some time interval that is determined by matching the part over which Y grows, during the upper phase of the liquid pendulum, to its oscillatory, relaxational decay part of the next cycle, during which the pendulum is in the lower half plane, and during which it will slowly ascend again (under the influence of heating).

The advantange of the present derivation over that cast in polar coordinates r, θ, as in van der Schrier and Maas (2000), is that we do not need an additional matching near the origin $(Y, Z) \approx (0, 0)$ (where θ "jumps" by π). Also, there is no additional approximation involved, as in that study, where $\sin\theta$ was replaced by $\pm\theta$. This approximation is appropriate for θ close to 0 or π, but was, in fact, applied also for θ near $\pm\pi/2$, motivated by the fact that the ascent and descent of the liquid pendulum occur on widely differing time scales. The ascent (θ near $0, \pi$) is a slow process, and the descent ($\theta \approx \pm\pi/2$) a very rapid process. Presently, the only problem is to decide exactly when to match. For this we choose the moment $T = Rt$ at which the liquid pendulum no longer grows in length. This occurs when $Y = Y_{max}$, or when $Z = 0$. From (25) it follows that $r \equiv (Y^2 + Z^2)^{1/2} \approx T$.

Thus, at $Z = 0$, $Y_{max} = sT$, where $s = \text{sign}(Y)$. Hence, the moment of matching is determined by finding the root of $Y = \dot{L} + L = sT$. Since the Ai/Bi-functions and their derivatives (indicated by primes) decrease/grow exponentially for a positive argument, only the Bi-function and its derivative are taken into account, $s = \text{sign}(\beta)$, and the time of matching T is determined by solving

$$e^{-\frac{T}{2R}}\beta(\delta \mathrm{Bi}'_+ + \frac{1}{2}\mathrm{Bi}_+) = sT. \tag{B4}$$

The arguments of the Airy functions $\mathrm{Ai}_\pm, \mathrm{Bi}_\pm$ are labelled by subscripts $\pm$, which are given by $(1/4 \pm T)\delta^{-2}$. Once T is known, we match L and $\dot{L}$ for the increasing part, to the oscillatory decay part of the next cycle, when angular momentum is lost by mechanical friction. This part of the solution is again given by (B3), except that it employs a shifted time $t' = t + 2T/R$, matching occurring at $t' = -T/R$. The undetermined amplitudes in the next cycle, denoted by primes, then follow from the matching conditions, and read

$$(\alpha', \beta') = \pi\beta e^{-T/R}(\mathrm{Bi}'_-\mathrm{Bi}_+ - \mathrm{Bi}'_+\mathrm{Bi}_-, \mathrm{Bi}'_+\mathrm{Ai}_- - \mathrm{Bi}_+\mathrm{Ai}'_-). \tag{B5}$$

Note that the dependence on α is lost owing to a multiplication with the vanishingly small Ai_+ or its derivative. In another application of (B4) (to primed quantities), β' now determines the positive time T' and therefore the maximum length which the pendulum reaches in the next cycle. To obtain an explicit approximate relation of T on β (and hence also of T' on β'), we use the asymptotic expansions of the Airy functions [Abramowitz and Stegun, (1965)],

$$\lim_{z\to\infty}(\mathrm{Bi}(z), \mathrm{Bi}'(z)) \to \pi^{-1/2}e^{\zeta}(z^{-1/4}, z^{1/4}), \tag{B6}$$

where

$$\zeta = \frac{2}{3}z^{3/2}, \tag{B7}$$

and argument

$$z = \delta^{-2}(T + \frac{1}{4}). \tag{B8}$$

Inserting these in the primed version of (B4) leads to

$$e^{\zeta'-T'/2R}=\frac{\pi^{1/2}sT'}{\delta^{1/2}\beta'}\left[\left(T'+\frac{1}{4}\right)^{1/4}+\frac{1}{2}\left(T'+\frac{1}{4}\right)^{-1/4}\right]^{-1}. \tag{B9}$$

Taking the logarithm of both sides, using the auxiliary variable $\eta'=(T'+1/4)^{1/2}$, gives

$$\frac{2}{3}\eta'^3-\frac{1}{2}\eta'^2-R\ln[\eta'^{1/2}(\eta'-1/2)]=R\ln[(\pi/\delta)^{1/2}/|\beta'|]-\frac{1}{8}\equiv p, \tag{B10}$$

Inserting β' into this equation from (B5), and from (B4), writing

$$\beta=sTe^{\frac{T}{2R}}(\delta\mathrm{Bi}'_{+}+\frac{1}{2}\mathrm{Bi}_{+})^{-1}, \tag{B11}$$

its right hand side p can be rewritten as

$$p(T)=\frac{T}{2}-\frac{1}{8}-R\ln\left[(\pi\delta)^{1/2}\left|T\mathrm{Ai}_{-}\,\frac{\mathrm{Bi}'_{+}/\mathrm{Bi}_{+}-\mathrm{Ai}'_{-}/\mathrm{Ai}_{-}}{\delta\mathrm{Bi}'_{+}/\mathrm{Bi}_{+}+1/2}\right|\right]. \tag{B12}$$

The left hand side of (B10) is a function of T', the right hand side, p, a function of T, given by (B12). Hence, solving for $\eta'=\eta'_0+R\eta'_1+\cdots$ as a function of $p(T)$ establishes the desired explicit relation (approximately)

$$T'(T)=-1/4+(\eta'_0+R\eta'_1+O(R^2))^2, \tag{B13}$$

where

$$\eta'_0=\frac{1}{2}\cosh(\cosh^{-1}(|48p+1|)/3)+\frac{1}{4}, \tag{B14}$$

and η_1' can be cast in terms of η_0'

$$\eta_1'=\ln[\eta_0'(\eta_0'-1/2)^2]/(2(2\eta_0'-1)\eta_0'). \tag{B15}$$

From (B12) it is evident that the map $T'(T)$ will have peaks ($T'\to\infty$) when the argument of the logarithm vanishes. Employing the asymptotic expansions

$$\lim_{z\to\infty}(\mathrm{Ai}(-z),\mathrm{Ai}'(-z))\to\pi^{-1/2}(\sin(\zeta+\pi/4)z^{-1/4},\cos(\zeta+\pi/4)z^{1/4}), \tag{B16}$$

applied to $z_- = \delta^{-2}(T - 1/4)$, where $\zeta_- = (2/3)z_-^{3/2}$, leads to

$$p = \frac{T}{2} - \frac{1}{8} - R \ln \left[\left| \frac{2T^2}{(T-1/4)^{1/4}((T+1/4)^{1/2} + 1/2)} \cos(\zeta_- + \pi/4 - \phi) \right| \right], \tag{B17}$$

where

$$\phi = \tan^{-1} \left(\frac{T + 1/4}{T - 1/4} \right)^{1/2}. \tag{B18}$$

Thus, the peaks are found at the zeros of the cosine, i.e., at

$$\zeta_- - \phi = (n + 1/4)\pi, \quad n = 1, 2, \ldots, \tag{B19}$$

which, for large T, occur at

$$T_n \approx \frac{1}{4} + \left(\frac{3}{4} R(2n-1)\pi \right)^{2/3}, \quad n = 1, 2, \ldots \tag{B20}$$

For $R = 0.1$, the solid curve of Figure 8 presents the analytical map (B13) up to order R^2, the dots represent numerically determined values by directly integrating the diffusionless Lorenz equations (23)–(25). The distances between subsequent peaks and the location of the baseline curve seem to be correct. The peak locations are closer to the numerical observations than to those given by van der Schrier and Maas (2000), but they still need further improvement.

References

Abramowitz, M. and Stegun, I. A.: 1965, *Handbook of Mathematical Functions,* Dover.

Arnold, L., Imkeller, P., and Wu, Y.: 2003, 'Reduction of Deterministic Coupled Atmosphere-ocean Models to Stochastic Ocean Models: A Numerical Case Study of the Lorenz-Maas System', *Dynamical Systems* **18,** 295–350.

Chandrasekhar, S.: 1968, *Ellipsoidal Figures of Equilibrium*, Yale Univ.

Dolzhanskiy, F. V.: 1977, 'On the Hydrodynamic Interpretation of the Equations of Motion of a Heavy Top', *Izv. Atmos Oc. Phys.* **13,** 140–142.

Dolzhanskiy, F. V. and Pleshanova, L. A.: 1983, 'Self-oscillations and Instability Phenomena in an Elementary Model of Convection', *Izv. Atmos. Oc. Phys.* **15,** 10–17.

Fisher, H. B., List, E. J., Koh, R. C. Y., Imberger, J., and Brooks, N. H.: 1979, *Mixing in Inland and Coastal Waters*, Academic Press.

Fowler A. C. and McGuinness, M. J.:1982, 'A Description of the Lorenz Attractor at High Prandtl Number', *Phys. D*, **5,** 149–182.
Fowler A. C. and McGuinness, M. J.: 1983, 'Hysteresis, Period Doubling, and Intermittency at High Prandtl Number in the Lorenz Equations', *Stud. Appl. Math.* **69,** 99–126.
Glendenning, P. and Sparrow, C.: 1984, 'Local and Global Behavior Near Homoclinic Orbits', *J. Stat. Phys.* **35,** 645–697.
Gluhovsky, A. B.: 1978, 'Modeling Turbulence by Systems of Coupled Gyrostats', in N. Fitzmaurice et al. (eds.), *Nonlinear Waves and Weak Turbulence*, Birkhauser.
Gluhovsky, A. and Agee, E.: 1977, 'An Interpretation of Atmospheric Low-order Models', *J. Atmos. Sci.* **54,** 768–773.
Gluhovsky, A. B. and Dolzhanskiy, F. V.: 1980, 'Three-component Geostrophic Models of Convection in a Rotating Fluid [Engl. Transl.]', *Izv. Atmos. Oc. Phys* **16,** 311–318.
Holm, D.: 1978, 'Gyroscopic Analog for Collective Motion of a Stratified Fluid', *J. Math. Anal. Appl.* **117,** 57–80.
Lesieur, M.: 1996, *Turbulence in Fluids*, 3rd ed., Kluwer Academic Publisher.
Lorenz, E. N.: 1960, 'Maximum Simplification of Dynamic Equations',*Tellus* **12,** 243–254.
Lorenz, E. N.: 1963, 'Deterministic Non-periodic Flow', *J. Atmos. Sci.* **20,** 130–141.
Lorenz, E. N.: 1979, 'On the prevalence of aperiodicity in simple systems', in M. Grmela and J. E. Marsden (eds.), *Global Analysis*, Springer.
Lorenz, E. N.: 1984, 'Irregularity: A Fundamental Property of the Atmosphere', *Tellus* **36A,** 98–110.
Lorenz, E. N.: 1990, 'Can Chaos and Intransitivity Lead to Interannual Variability'?, *Tellus* **42A,** 378–389.
Maas, L. R. M.: 1994, 'A Simple Model for the Three-dimensional, Thermally and Wind-driven Ocean Circulation', *Tellus* **46A,** 671–680.
Maas, L. R. M. and van Haren, J. J. M.: 1987, 'Observations on the Vertical Structure of Tidal and Inertial Currents in the Central North Sea', *J. Marine Res.* **45,** 293–318.
Monahan, A. H.: 2002, 'Lyapunov Exponents of a Simple Stochastic Model of the Thermally and Wind-driven Ocean Circulation', *Dyn. Atmos. Oc.* **35,** 363–388.
Morgan, G. W.: 1956, 'On the Wind-driven Ocean Circulation', *Tellus* **8,** 95–114.
Mullin, T. and Price, T. J.: 1989, 'An Experimental Observation of Chaos Arising from the Interaction of Steady and Time-dependent Flow', *Nature* **340,** 294–296.
Obukhov, A. M.: 1969, 'Integral Invariants in Hydrodynamic Systems', *Dokl. Akad. Nauk SSSR* **14,** 32–35.
Obukhov, A. M. and Dolzhansky, F. V.: 1975, 'On Simple Models for Simulation of Nonlinear Processes in Convection and Turbulence', *Geophys. Fluid Dyn.* **6,** 195–209.
Olbers, D. A: 2001, 'Gallery of Simple Models', in: P. Imkeller and J. S. von Storch, (eds.), *Progress in Probability 49*, Birkhaeuser Verlag.
Rutgers, M. A.: 1998, 'Forced 2D Turbulence: Experimental Evidence of Simultaneous Inverse Energy and Forward Enstrophy Cascades', *Phys. Rev. Lett.* **81,** 2244–2247.
Sommeria, J.: 1986, 'Experimental Study of the Two-dimensional Inverse Energy Cascade in a Square Box', *J. Fluid Mech.* **170,** 139–168.
Sparrow, C.: 1982, *The Lorenz Equations: Bifurcations, Chaos and Strange attractors.* Springer.
Staquet, C.: 2000, 'Mixing in a Stably Stratified Shear Layer: Two- and Three-Dimensional Numerical Experiments', *Fluid Dyn. Res.* **27,** 367–404.
Stommel, H.: 1961, 'Thermohaline convection with two stable regimes of flow', *Tellus* **13,** 224–230.
van der, Schrier, G.: 2000, 'Aspects of the Thermohaline Circulation in a Simple Model', Ph.D Thesis', Utrecht University, 110 pp.

van der, Schrier, G. and Maas, L. R. M.: 1998, 'Chaos in a Simple Model of the Three-dimensional Salt-dominated Ocean Circulation', *Climate Dynamics* **14,** 489–502.

van der, Schrier, G. and Maas, L. R. M.: 2000, 'The Diffusionless Lorenz Equations: Shil'nikov Bifurcations and Reduction to an Explicit Map', *Phys. D* **141,** 19–36.

van Veen, L.: 2002, 'Time Scale Interaction in Low-order Climate Models', Ph.D Thesis, Utrecht University, 89 pp.

van Veen, L., Opsteegh, T. and Verhulst F.: 2004, Overturning and Wind-driven Circulation in a Low-order Ocean-atmosphere Model. Submitted to *Dyn. Atm. OC*.

Wunsch, C. and Stammer D.: 1997, 'Atmospheric Loading and the Oceanic "Inverted Barometer" Effect', *Rev. Geophys.* **35,** 79–107.

Zaslavsky, G. M., Sagdeev, R. Z., Usikov D. A., and Chernikov, A. A.: 1991, *Weak Chaos and Quasi-Regular Patterns*, Cambridge University Press.